Science
AAAS

Ultrasmooth Patterned Metals for Plasmonics and Metamaterials
Prashant Nagpal, *et al.*
Science **325**, 594 (2009);
DOI: 10.1126/science.1174655

Science (print ISSN 0036-8075; online ISSN 1095-9203) is published weekly, except the last week in December, by the American Association for the Advancement of Science, 1200 New York Avenue NW, Washington, DC 20005.

Ultrasmooth Patterned Metals for Plasmonics and Metamaterials

Prashant Nagpal,[1] Nathan C. Lindquist,[2] Sang-Hyun Oh,[2] David J. Norris[1]*

Surface plasmons are electromagnetic waves that can exist at metal interfaces because of coupling between light and free electrons. Restricted to travel along the interface, these waves can be channeled, concentrated, or otherwise manipulated by surface patterning. However, because surface roughness and other inhomogeneities have so far limited surface-plasmon propagation in real plasmonic devices, simple high-throughput methods are needed to fabricate high-quality patterned metals. We combined template stripping with precisely patterned silicon substrates to obtain ultrasmooth pure metal films with grooves, bumps, pyramids, ridges, and holes. Measured surface-plasmon–propagation lengths on the resulting surfaces approach theoretical values for perfectly flat films. With the use of our method, we demonstrated structures that exhibit Raman scattering enhancements above 10^7 for sensing applications and multilayer films for optical metamaterials.

Plasmonic devices exploit electromagnetic waves known as surface plasmons that can propagate along a metal interface (*1*). Because these waves involve a mixture of both light and charge fluctuations on the metal surface, they have a unique hybrid character. Their photonic component allows them to interact with optical waves, whereas their electronic component allows these optical waves to be concentrated in volumes much smaller than the diffraction limit. This combination is useful for applications ranging from biosensing to solar cells (*2*–*6*). In a typical device, surface plasmons are created when a film of silver or gold is illuminated on its exposed surface. Although this excitation process is forbidden when the interface is perfectly flat, surface patterning on a suboptical length scale allows incident light to generate surface plasmons in the film (*1*). Patterning also provides a means to manipulate these plasmons, once they have been created. For example, surface structures can direct, channel, or focus the surface plasmons toward specific locations. However, because surface plasmons exist very close to the interface, they are extremely sensitive to surface inhomogeneities, which can cause absorption, scattering, and limited propagation. Consequently, fabrication of plasmonic devices requires metal films to be patterned while avoiding unwanted roughness and impurities that can seriously degrade their performance.

Unfortunately, metal films deposited by evaporation are inherently rough due to polycrystallinity. Moreover, when such films are patterned, for example by a focused ion beam (FIB), this roughness is increased as the grains are exposed. To avoid these problems, alternatives ranging from films with extremely small grains grown by fast sputtering (*7*) to large single crystals grown by the Czochralski process (*8*, *9*) have been explored. Although each of these alternatives can provide surfaces that are smoother than evaporated films, their devices still exhibit shorter-than-expected surface-plasmon propagation. In particular, ion impurities implanted in the metal during patterning introduce absorption. For sputtered films, plasmons can also scatter at the numerous grain boundaries. To increase the propagation, one solution is to use extremely thin metal films (~10 nm), in which long-range surface plasmons have been reported at infrared wavelengths (*10*). However, this occurs because most of the electromagnetic field from the surface plasmon is in the surrounding medium instead of the metal. For applications that exploit concentrated electromagnetic fields near a metal interface, thicker structures are required. All fabrication methods have also been limited to patterning one film at a time. This affects not only cost but also performance, because nanometer-scale differences between structures can influence the plasmons.

The emerging field of plasmonics needs simple, high-throughput, and reproducible approaches to obtain pure metallic films that are smooth yet patterned over large areas. Although techniques such as nanoimprinting and nanomolding can easily pattern metals on the proper length scales (*11*–*13*), none of these methods have been suitable. In most techniques, patterned polymeric molds are filled with metal to form a replica. This process introduces serious surface roughness because metals do not easily wet polymer interfaces. Even if this problem is avoided by substituting other mold materials, molds have to be etched away to release the metal structure. This reduces throughput and reproducibility because each mold generates only one device.

In contrast, a simple technique already exists to generate smooth unpatterned metallic films. Known as template stripping, this method makes use of the poor adhesion and good wettability of noble metals on solids such as mica, glass, and silicon (*14*). Typically, freshly cleaved mica is coated with a film of gold, and the exposed surface of gold is then attached to another substrate with an epoxy adhesive. When the mica and substrate are separated, the gold clings to the epoxy, and a metal interface that has formed on the mica is exposed. Because mica can be extremely smooth, ultraflat gold surfaces can be generated. These have been used widely in scanning probe experiments and studies of self-assembled monolayers.

However, it has not been realized that the same approach can produce smooth patterned metal films. Whereas template stripping was applied to form patterns on mica, complex multistep processes were employed (*15*–*17*). Instead of mica, we used inexpensive silicon wafers as the template to exploit the well-developed fabrication techniques for microelectronics. After the wafer is patterned (Fig. 1A), for example, with lithography or FIB, it is coated with a thin metal film and a layer of epoxy (*18*). The epoxy-metal bilayer can then be peeled off of the substrate to reveal a patterned structure with a surface roughness determined by the wafer template. Figure 1B shows a silicon substrate with circular concentric grooves defined by FIB. We thermally evaporated 275 nm of silver on this substrate, added epoxy, and peeled off the bilayer. Figure 1, C to E, indicates the quality of the silver "bull's eye" structure that results. Electron micrographs taken at glancing incidence (Fig. 1E) are extremely effective at exposing any surface roughness.

The evaporated silver film has a rough surface after deposition, but the device uses the opposite interface, which is smooth. If the film is thicker than ~100 nm, the rough side will not influence surface-plasmon propagation. Because the silicon wafer, and not the silver, is patterned by FIB or reactive ion etching (RIE), no ion impurities are implanted in the silver. We used x-ray photoelectron spectroscopy to analyze the surface composition of metal films patterned via RIE with SF_6 and found 49 atomic percent of fluoride ions within the top ~5 nm of the film, whereas template-stripped metals had no detectable surface impurities.

In addition to silver bull's eyes, we fabricated a variety of silver, copper, and gold plasmonic structures (Fig. 2). From the same patterned substrate, we have created more than 30 films without damage. If it was necessary to avoid epoxy, which remains attached to the metal and can be problematic for some applications, we used metal electrodeposition (*19*). For example, after a thin ~250-nm film of copper was evaporated onto a bull's eye template, we electrodeposited another ~1 mm of copper. The resulting patterned copper foil (Fig. 2A) could be peeled off directly, without the aid of epoxy. Similarly, a silver bump array (Fig. 2B) was produced on a free-standing ~100-μm-thick silver foil.

We also used simple chemical etching techniques to pattern the silicon substrate. When the surface of a [100]-oriented silicon wafer is exposed to a solution of KOH, anisotropic etching can lead to pyramidal divets or triangular grooves. We formed such patterns by coating a

[1]Department of Chemical Engineering and Materials Science, University of Minnesota, Minneapolis, MN 55455, USA. [2]Department of Electrical and Computer Engineering, University of Minnesota, Minneapolis, MN 55455, USA.

*To whom correspondence should be addressed. E-mail: dnorris@umn.edu

wafer with chromium and gold, selectively removing these layers with either FIB or photolithography, and immersing the substrate in KOH (*18*). Previously, pyramidal particles were created by depositing metals only at the bottom of such divets and then releasing the deposits to form a colloidal suspension (*20*, *21*). In our case, the divets were coated with ~250 nm of metal, which was removed with epoxy to produce silver (Fig. 2, C and D) or gold (Fig. 2E) pyramid arrays. (We also obtained similar structures with electrodeposition.) The pyramids were smooth, highly reproducible, and exhibited sharp tips with radii of curvature as small as 10 nm (Fig. 2D, inset).

The surfaces that are produced have a roughness that can approach that of the template, as confirmed by atomic force microscopy (AFM). For a silicon substrate with a root mean square (RMS) roughness of 0.19 nm, we measured 0.65 nm for the corresponding silver film. The largest contribution to this value was the grain boundaries in the polycrystalline silver. Within a single grain, the roughness was 0.26 nm, much closer to that of the silicon. These measurements were obtained for silver evaporated onto test-grade wafers at room temperature (*18*). Under slow-evaporation conditions with wafers heated to 75°C, the RMS roughness improved even further to 0.34 nm. Of course, the smoothness of the metal is affected by the method that we used to pattern the substrate. For example, the silicon bull's eye in Fig. 1B had an RMS roughness of 1.89 nm due to redeposition of material during patterning of the grooves with FIB. The corresponding silver film (Fig. 1C) had a roughness of 2.18 nm. Even in this case, the bull's eye, which is designed to have a sharp and directional absorption feature due to optical coupling to surface plasmons, exhibited a sharp absorption peak (fig. S1) that was not observed in the same structure made by standard methods (i.e., evaporated films patterned directly with FIB).

To quantify this further, we measured the propagation length of the surface plasmons. We prepared a 200-nm-thick ultrasmooth silver film on epoxy and then milled a series of identical slits through the metal with FIB. For each slit, we added a parallel groove in the film at a different fixed separation *d* (Fig. 3A). By illuminating the epoxy side of the bilayer with white light, surface plasmons could be launched on the film as light passed through the slits (*22*). When these propagating plasmons struck the grooves (Fig. 3A, inset), they scattered light that could be collected by a microscope. For each groove, we measured the spectrum of this light and, from an analysis of all such spectra, determined the scattered intensity as a function of *d*. Because this is directly related to the intensity of the surface plasmons at the

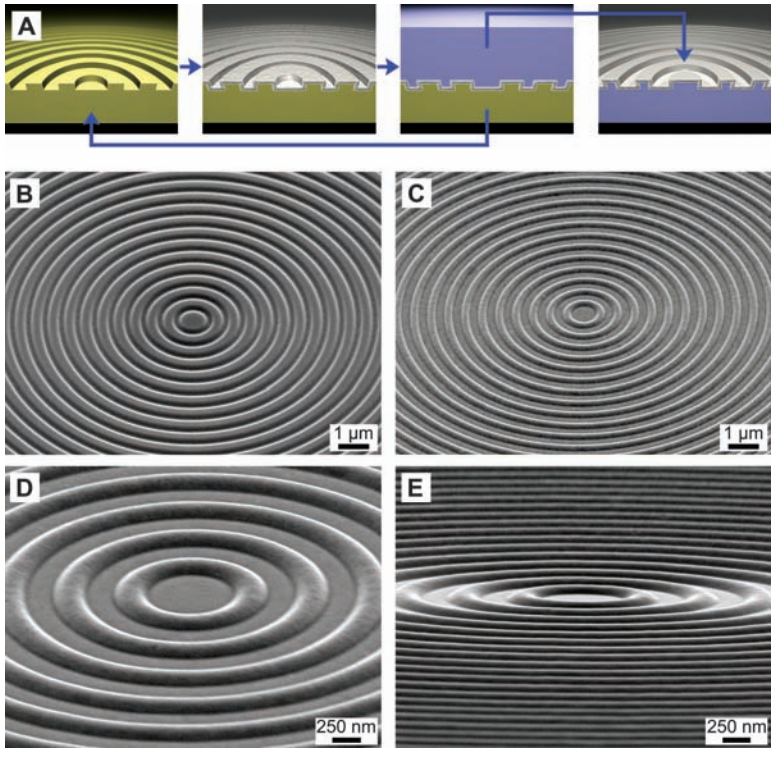

Fig. 1. (**A**) Schematic for fabricating ultrasmooth patterned plasmonic structures. After adding a desired pattern to a silicon wafer (green), a metal film is deposited and then coated with epoxy or additional metal (blue). The combined film can be peeled off of the substrate to reveal a smooth patterned surface. The substrate can be reused to form additional identical structures. (**B**) Electron micrograph of a silicon wafer patterned with circular grooves (bull's eye) by FIB. The grooves were 285 nm wide and spaced every 570 nm. (**C** to **E**) Electron micrographs of a silver bull's eye that was template stripped off of the silicon substrate in (B) using epoxy.

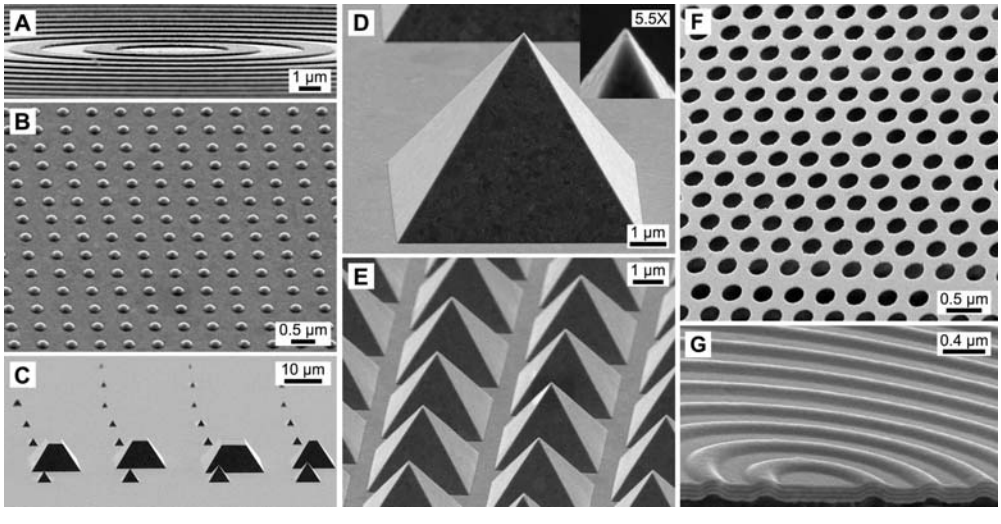

Fig. 2. Electron micrographs of various metal structures. (**A**) A copper bull's eye with 1.3-μm-wide circular grooves spaced every 3.5 μm; the template was patterned with photolithography and RIE. (**B**) A square silver array of 240-nm-diameter bumps spaced every 600 nm; the template was patterned with FIB. (**C** and **D**) A silver pyramid array made by anisotropic etching. A gold-on-chromium mask with square holes was formed with FIB on a silicon wafer and etched in KOH. The inset in (D) shows the tip of one of the pyramids. (**E**) A gold pyramid array made by anisotropic etching as in (C), except a chromium mask was patterned with a hexagonal array of 1-μm-diameter circles spaced by 2.25 μm using photolithography. (**F**) A thin silver nanohole array made with template stripping and nanosphere lithography. 265-nm-diameter holes spaced by 450 nm were formed in a 30-nm-thick silver film. (**G**) A multilayer bull's eye with alternating layers of silver (30 nm) and alumina (15 nm). A cross section etched by FIB shows seven layers.

grooves, the plasmon propagation length could be extracted for each wavelength. Figure 3B shows the measured propagation lengths for our template-stripped film. [Fringes appear in these data because of interference between surface plasmons propagating toward and away from the groove (*22*).] For comparison, we also plotted previously reported propagation lengths (*23*), as well as those that we obtained for a control film made by standard methods.

Due to roughness, propagating surface plasmons can be scattered in-plane (into other surface plasmons) or out-of-plane (into light). These losses can be quantified individually by propagation lengths L_{scat} and L_{rad}, respectively, that contribute to the overall propagation length L_{tot} (*1*, *24*). For a perfectly smooth single-crystalline film, L_{scat} and L_{rad} are infinite, and L_{tot} is limited by the ohmic losses (electron scattering) in the metal, described by L_{ohm}. If the dielectric properties of the film are known, L_{ohm} can be calculated directly (*18*). Using ellipsometry, we measured the dielectric function for our films and computed L_{ohm} (see figs. S2, S3, and S4). Figure 3B illustrates a comparison of our slit-groove data with L_{ohm} determined for a template-stripped film exposed to the same conditions. The measured values are close to L_{ohm}, especially at longer wavelengths.

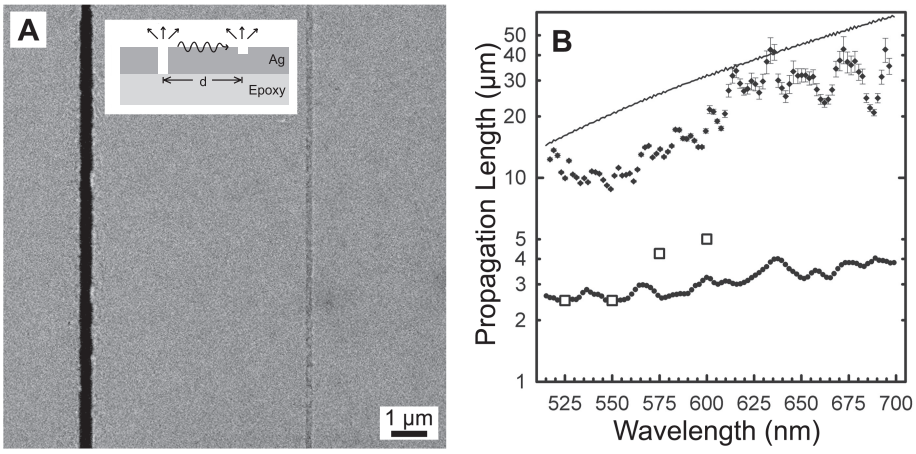

Fig. 3. (**A**) An electron micrograph of a slit-groove pair separated by 6 μm in a template-stripped 200-nm-thick silver (Ag) film. (**B**) Plot of propagation length versus wavelength extracted from a range of slit-groove separations, *d*. At every wavelength, we fit the decay of the scattered intensity with an exponential to extract the propagation length (diamonds). Error bars denote SE. Fringes appear in these data because of interference of surface plasmons propagating toward the groove and those reflected back, as confirmed by finite difference time-domain simulations. From the measured dielectric function of a template-stripped silver film treated to the same conditions, we determined the expected propagation length assuming only ohmic losses (solid curve) (*1*). Previously reported data (squares) (*23*) and values extracted from the rough side of a thermally evaporated control film (circles) are also shown. Error bars for the control data were smaller than the symbols in the plot and are not shown.

To confirm that the observed increase in propagation length is due to decreased roughness, we combined AFM and ellipsometry data to estimate the effect of different contributions to L_{tot} for template-stripped silver and gold samples, as well as standard films (*18*). From AFM scans (figs. S5 and S6), parameters describing the surface corrugation could be extracted (table S1) and used to estimate L_{scat} and L_{rad} within the single scattering approximation (*1*, *24*, *25*). L_{ohm} was determined separately from ellipsometry data. Table S2 shows that the reduction of surface roughness in template-stripped silver films should cause an increase in L_{tot} by a factor of 5 to 7, in agreement with Fig. 3B. For gold, which is inherently smoother than silver, the improvement is smaller. However, other benefits of template stripping may still be exploited. AFM scans (figs. S5 and S6) suggest a large increase in the grain size for template-stripped films. This occurred in silver during the mild heat treatment that we used to cure the epoxy (150°C). In gold, we intentionally annealed at 500°C. Unlike standard films, where thermal annealing under the same conditions increases roughness, template stripping allows grains to grow while constraining the surface. Because scattering of plasmons at grain boundaries can be an important loss mechanism on gold interfaces (*9*), grain growth can improve plasmon propagation. Assuming an increase in grain size from 80 to 1000 nm (fig. S6), L_{tot} should be improved by a factor of ~2 (table S3). The combined effect of larger grains, decreased roughness, and reduced impurities should also increase L_{ohm} due to reduced electron scattering. This increase and the preferred grain orientation (texturing) that we observe on template-stripped films offer additional advantages.

To demonstrate the utility of our approach, we fabricated large-area (square centimeters) substrates for surface-enhanced Raman scattering (SERS). In general, Raman scattering can identify molecules through their unique vibrational signatures. Because of the concentrated electric fields near patterned metal surfaces, gold and silver films have been studied for enhanced molecular and biological sensing (*26*). Signal enhancements above 10^8 for specific surface structures have been reported (*27*). However, more important for sensing applications is the ability to generate enhancements with films that are easily and reproducibly fabricated, and we illustrate this ability in Fig. 4. We first formed triangular grooves on a silicon wafer by combining photolithography and anisotropic etching (Fig. 4A). Figure 4B shows the smooth silver film with raised triangular ridges that was peeled off of this wafer. We then attached a self-assembled monolayer of benzenethiol to this surface and used scanning confocal Raman microscopy to collect the SERS signal as a function of position. The

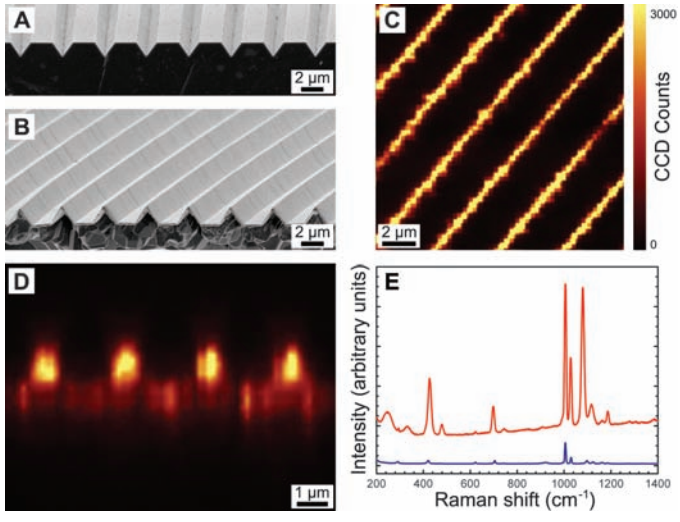

Fig. 4. (**A**) Electron micrograph of a silicon wafer patterned with a grating of triangular grooves by photolithography, lift-off, and anisotropic etching. The grooves cover 2 × 2 cm^2 on the wafer. (**B**) A silver film with triangular ridges formed from the wafer in (A). 280 nm of silver was evaporated, followed by 100 μm by electrodeposition. Due to slight misalignment of the grooves and the <110> direction of the wafer, step edges formed in the grooves during etching that are reproduced on the sides of the silver ridges. (**C** and **D**) Confocal Raman scattering microscopy scans of the film in (B) after incubation in 1 mM benzenethiol in ethanol for 16 hours. The excitation wavelength was 514 nm. The scan was in the plane of the ridge peaks in (C) and a cross section of the ridges in (D). CCD, charge-coupled device. (**E**) Raman scattering spectra for the same benzenethiol-coated silver film shown in (C) and (D) (red curve) and for neat benzenethiol (blue curve). The excitation wavelength was 532 nm.

resulting images for scans parallel to the ridge tops (Fig. 4C) reveal uniformly enhanced signals near the triangular peaks. More importantly, cross-sectional scans (Fig. 4D) show that the response is high at this peak while remaining low along the smooth sides of the ridges and the valleys in between. Using the protocol and apparatus in (*28*), we quantified the SERS enhancement by comparing the Raman signal from neat benzenethiol with that from our monolayer-coated substrate (Fig. 4E). After correcting for the number of molecules, we determined an enhancement factor of 1.4×10^7. Because this represents an average over the entire surface, the actual enhancement near the ridge peak should be much higher.

Whereas bumps, ridges, and grooves are clearly useful for these types of applications, different structural elements are necessary for others. For example, a nanoscale hole surrounded by surface structures can allow enhanced transmission of electromagnetic waves through a metal film (*3*). Figure 2F shows that we can also create such holes in thin smooth silver films. A hexagonal array of deep circular pits was formed on a silicon wafer with nanosphere lithography. By evaporating silver on top of such pits and adding epoxy, a thin silver film with a hole array was obtained. Although only one side of this film is ultrasmooth, which would affect its transmission properties, an additional absorbing layer such as Cr could be added to the rough side to minimize its effects. A second useful element is the multilayer structure. For example, thin patterned films with alternating layers of metal and insulator can exhibit a negative refractive index (*29*), which can lead to new optical phenomena (*30*). Our approach can also yield such structures, called metamaterials. After evaporating a thin film of silver on patterned silicon templates, we deposited alternating layers of alumina and silver. Because silver adheres to alumina better than silicon, the entire stack could be removed with epoxy. For example, a bull's eye (Fig. 2G) and a bump array (fig. S7) could be easily obtained, both of which have potential use as superlenses (*30*). As long as the adhesion requirement is satisfied, other materials besides alumina are also possible. The resulting films can lead to a variety of useful optoelectronic devices, especially considering that they are formed on flexible substrates with built-in metal contacts.

These results indicate that template stripping can be combined with silicon microfabrication methods to create ultrasmooth patterned metals for plasmonics and metamaterials. Although extremely simple, it provides a route to fabricate integrated metallic multilayer structures with designed grooves, bumps, tips, and holes with controlled spacings and orientations, while simultaneously avoiding previous problems because of roughness and impurities.

References and Notes

1. H. Raether, *Surface Plasmons* (Springer, Berlin, 1988).
2. H. A. Atwater, *Sci. Am.* **296**, 56 (2007).
3. C. Genet, T. W. Ebbesen, *Nature* **445**, 39 (2007).
4. E. Ozbay, *Science* **311**, 189 (2006).
5. N. Engheta, *Science* **317**, 1698 (2007).
6. A. Polman, *Science* **322**, 868 (2008).
7. L. Yin *et al.*, *Nano Lett.* **5**, 1399 (2005).
8. E. J. R. Vesseur *et al.*, *Appl. Phys. Lett.* **92**, 083110 (2008).
9. M. Kuttge *et al.*, *Appl. Phys. Lett.* **93**, 113110 (2008).
10. D. Sarid, *Phys. Rev. Lett.* **47**, 1927 (1981).
11. B. D. Gates *et al.*, *Chem. Rev.* **105**, 1171 (2005).
12. Y. L. Loo, R. L. Willett, K. W. Baldwin, J. A. Rogers, *J. Am. Chem. Soc.* **124**, 7654 (2002).
13. G. Kumar, H. X. Tang, J. Schroers, *Nature* **457**, 868 (2009).
14. M. Hegner, P. Wagner, G. Semenza, *Surf. Sci.* **291**, 39 (1993).
15. M. Graca, J. Turner, M. Marshall, S. Granick, *J. Appl. Phys.* **102**, 064909 (2007).
16. B. Jung, W. Frey, *Nanotechnology* **19**, 145303 (2008).
17. W. Frey, C. K. Woods, A. Chilkoti, *Adv. Mater.* **12**, 1515 (2000).
18. See supporting material on *Science* Online.
19. P. Samori, J. Diebel, H. Lowe, J. P. Rabe, *Langmuir* **15**, 2592 (1999).
20. Q. B. Xu, I. Tonks, M. J. Fuerstman, J. C. Love, G. M. Whitesides, *Nano Lett.* **4**, 2509 (2004).
21. J. Henzie, E. S. Kwak, T. W. Odom, *Nano Lett.* **5**, 1199 (2005).
22. V. V. Temnov, U. Woggon, J. Dintinger, E. Devaux, T. W. Ebbesen, *Opt. Lett.* **32**, 1235 (2007).
23. J. T. van Wijngaarden *et al.*, *Appl. Phys. Lett.* **88**, 221111 (2006).
24. D. L. Mills, *Phys. Rev. B* **12**, 4036 (1975).
25. H. Shiba, M. Haraguchi, M. Fukui, *J. Phys. Soc. Jpn.* **63**, 1400 (1994).
26. A. J. Haes *et al.*, *MRS Bull.* **30**, 368 (2005).
27. C. L. Haynes, R. P. Van Duyne, *J. Phys. Chem. B* **107**, 7426 (2003).
28. K. C. Bantz, C. L. Haynes, *Langmuir* **24**, 5862 (2008).
29. G. Dolling, M. Wegener, S. Linden, *Opt. Lett.* **32**, 551 (2007).
30. D. R. Smith, J. B. Pendry, M. C. K. Wiltshire, *Science* **305**, 788 (2004).

31. We thank K. Bantz and C. Haynes for help with SERS measurements and B. Carlson for help with x-ray photoelectron spectroscopy. This work was supported by the U.S. Department of Energy (grant DE-FG02-06ER46438) and used resources in the Institute of Technology at the University of Minnesota, including the Nanofabrication Center, which receives partial support from NSF through the National Nanotechnology Infrastructure Network program, and the Characterization Facility, which has received capital equipment funding from NSF through the Materials Research Science and Engineering Center, Major Research Instrumentation, and Engineering Research Center programs. S.-H.O. acknowledges support from a Minnesota Partnership for Biotechnology Award and a 3M Non-Tenured Faculty Award. P.N. and N.C.L. acknowledge support from a University of Minnesota doctoral dissertation fellowship and an NIH Biotechnology training grant, respectively. The authors have applied for a patent on the fabrication methods described.

Supporting Online Material

www.sciencemag.org/cgi/content/full/325/5940/594/DC1
Materials and Methods
Figs. S1 to S7
Tables S1 to S3
References

7 April 2009; accepted 16 June 2009
10.1126/science.1174655

Probing Spin-Charge Separation in a Tomonaga-Luttinger Liquid

Y. Jompol,[1]* C. J. B. Ford,[1] J. P. Griffiths,[1] I. Farrer,[1] G. A. C. Jones,[1] D. Anderson,[1] D. A. Ritchie,[1] T. W. Silk,[2] A. J. Schofield[2]

In a one-dimensional (1D) system of interacting electrons, excitations of spin and charge travel at different speeds, according to the theory of a Tomonaga-Luttinger liquid (TLL) at low energies. However, the clear observation of this spin-charge separation is an ongoing challenge experimentally. We have fabricated an electrostatically gated 1D system in which we observe spin-charge separation and also the predicted power-law suppression of tunneling into the 1D system. The spin-charge separation persists even beyond the low-energy regime where the TLL approximation should hold. TLL effects should therefore also be important in similar, but shorter, electrostatically gated wires, where interaction effects are being studied extensively worldwide.

The effects of interactions are almost impossible to calculate in a general many-particle system, although they cannot be ignored. However, for a one-dimensional (1D) system, Luttinger, building on an approximation scheme of Tomonaga, constructed a soluble 1D model with infinite linear dispersion and a restricted set of interactions. The solution has the remarkable property that the excitations of spin and charge behave independently and move with different speeds. It has been argued (*1*) that all 1D metals are adiabatically continuous with the Tomonaga-Luttinger model at low energies, and hence spin-charge separation should be observable in real systems. Determining the extent of its applicability would provide a major test of more general methods of modeling interaction effects, with relevance to quantum devices and the theory of high-temperature superconductivity. Recent work (*2*) presents a more general theory of 1D systems with a nonlinear dispersion, but the effects of spin are not yet included.

Some properties of the Tomonaga-Luttinger liquid (TLL), such as power-law behavior, have been observed and studied in a variety of systems,

[1]Cavendish Laboratory, University of Cambridge, J. J. Thomson Avenue, Cambridge CB3 0HE, UK. [2]School of Physics and Astronomy, University of Birmingham, Edgbaston, Birmingham B15 2TT, UK.

*To whom correspondence should be addressed. E-mail: yodchay.jompol@cantab.net